MICROSCOPE Mission: First Results of a Space Test of the Equivalence Principle

Pierre Touboul,[1,*] Gilles Métris,[2,†] Manuel Rodrigues,[1,‡] Yves André,[3] Quentin Baghi,[2] Joël Bergé,[1] Damien Boulanger,[1] Stefanie Bremer,[4] Patrice Carle,[1] Ratana Chhun,[1] Bruno Christophe,[1] Valerio Cipolla,[3] Thibault Damour,[5] Pascale Danto,[3] Hansjoerg Dittus,[6] Pierre Fayet,[7] Bernard Foulon,[1] Claude Gageant,[1] Pierre-Yves Guidotti,[3] Daniel Hagedorn,[8] Emilie Hardy,[1] Phuong-Anh Huynh,[1] Henri Inchauspe,[1] Patrick Kayser,[1] Stéphanie Lala,[1] Claus Lämmerzahl,[4] Vincent Lebat,[1] Pierre Leseur,[1] Françoise Liorzou,[1] Meike List,[4] Frank Löffler,[8] Isabelle Panet,[9] Benjamin Pouilloux,[3] Pascal Prieur,[3] Alexandre Rebray,[1] Serge Reynaud,[10] Benny Rievers,[4] Alain Robert,[3] Hanns Selig,[4] Laura Serron,[2] Timothy Sumner,[11] Nicolas Tanguy,[1] and Pieter Visser[12]

[1]*ONERA, chemin de la Hunière, BP 80100, F-91123 Palaiseau Cedex, France*
[2]*Université Côte d'Azur, Observatoire de la Côte d'Azur, CNRS, IRD, Géoazur,*
250 Avenue Albert Einstein, F-06560 Valbonne, France
[3]*CNES, 18 avenue Edouard Belin, F-31401 Toulouse, France*
[4]*ZARM, Center of Applied Space Technology and Microgravity, University of Bremen,*
Am Fallturm, D-28359 Bremen, Germany
[5]*IHES, Institut des Hautes Études Scientifiques, 35 route de Chartres, F-91440 Bures-sur-Yvette, France*
[6]*DLR, Köln Headquarters, Linder Höhe, 51147 Köln, Germany*
[7]*LPTENS, École Normale Supérieure (PSL Research University), 24 Rue Lhomond, 75231 Paris Cedex 05, France*
[8]*PTB, Physikalisch-Technische Bundesanstalt, Bundesallee 100, 38116 Braunschweig, Germany*
[9]*IGN, Institut Géographique National, 73 Avenue de Paris, F-94160 Saint Mandé, France*
[10]*Laboratoire Kastler Brossel, UPMC-Sorbonne Université, CNRS,*
ENS-PSL Research University, Collège de France, F-75005 Paris, France
[11]*Blackett Laboratory, Imperial College London, United Kingdom*
[12]*Faculty of Aerospace Engineering, Delft University of Technology, Kluyverweg 1, 2629 HS Delft, The Netherlands*

According to the weak equivalence principle, all bodies should fall at the same rate in a gravitational field. The *MICROSCOPE* satellite, launched in April 2016, aims to test its validity at the 10^{-15} precision level, by measuring the force required to maintain two test masses (of titanium and platinum alloys) exactly in the same orbit. A nonvanishing result would correspond to a violation of the equivalence principle, or to the discovery of a new long-range force. Analysis of the first data gives $\delta(\mathrm{Ti}, \mathrm{Pt}) = [-1 \pm 9(\mathrm{stat}) \pm 9(\mathrm{syst})] \times 10^{-15}$ (1σ statistical uncertainty) for the titanium-platinum Eötvös parameter characterizing the relative difference in their free-fall accelerations.

Introduction.—Gravity seems to enjoy a remarkable universality property: bodies of different compositions fall at the same rate in an external gravitational field [1–3]. Einstein interpreted this as an equivalence between gravitation and inertia [4], and used this (weak) equivalence principle (WEP) as the starting point for the theory of general relativity [5]. In terms of the Eötvös parameter $\delta(A, B) = 2(a_A - a_B)/(a_A + a_B)$ (a_A and a_B being the free-fall accelerations of the two bodies A and B), the best laboratory (1σ) upper limits on $\delta(A, B)$ are $\delta(\mathrm{Be}, \mathrm{Ti}) = (0.3 \pm 1.8) \times 10^{-13}$ and $\delta(\mathrm{Be}, \mathrm{Al}) = (-0.7 \pm 1.3) \times 10^{-13}$ [2], with similar limits on the differential acceleration between Earth and the Moon toward the Sun [3].

General relativity (GR) has passed all historical and current experimental tests [6], including, most recently, the direct observation of the gravitational waves emitted by two coalescing black holes [7]. However, it does not provide a consistent quantum gravity landscape and leaves many questions unanswered, in particular about dark energy and the unification of all fundamental interactions. Possible avenues to close those problems may involve very weakly coupled new particles, such as the string-theory spin-0 dilaton [8,9], a chameleon [10], or a spin-1 boson U from an extended gauge group [11,12], generally leading to an apparent WEP violation.

The *MICROSCOPE* space mission implements a new approach to test the WEP by taking advantage of the very quiet space environment. Nongravitational forces acting on the satellite are counteracted by cold gas thrusters making it possible to compare the accelerations of two test masses of different compositions "freely falling" in the same orbit around Earth for a long period of time [13,14]. This is done by accurately measuring the force required to keep the two test masses in relative equilibrium. Present data allow us to improve the 1σ upper limit on the validity of the WEP by an order of magnitude.

The MICROSCOPE space mission.—*MICROSCOPE* aims to test the equivalence principle with an unprecedented

TABLE I.   Main test-mass physical properties measured in the laboratory before integration in the instrument.

Measured parameters at 20 °C	SUREF Inner mass Pt:Rh	SUREF Outer mass Pt:Rh	SUEP Inner mass Pt:Rh	SUEP Outer mass Ti:Al
Mass in kg	0.401 533	1.359 813	0.401 706	0.300 939
Density in g cm^{-3}	19.967	19.980	19.972	4.420

precision of 10^{-15}. The T-SAGE (Twin Space Accelerometers for Gravitation Experiment) scientific payload, provided by ONERA, is integrated within a CNES microsatellite. It was launched and injected into a 710 km altitude, circular orbit, by a Soyouz launcher from Kourou on April 25, 2016. The orbit is sun-synchronous, dawn-dusk (i.e., the ascending node stays at 18 h mean solar time) in order to have long eclipse-free periods (eclipses are defined as periods within Earth's shadow and happen only between May and July).

T-SAGE is composed of two parallel similar differential accelerometer instruments, each one with two concentric hollow cylindrical test masses. They are exactly the same, except for the use of different materials for the test masses. In one instrument (SUREF) the two test masses have the same composition, and are made from a platinum:rhodium alloy (90:10). In the other instrument (SUEP), the test masses have different compositions: Pt:Rh (90:10) for the inner test mass and titanium:aluminum:vanadium (90:6:4) (TA6V) for the outer test mass (see Table I). The test-mass shape has been designed to reduce the local self-gravity gradients due to multipole moment residues [15,16].

The test masses experience almost the same Earth gravity field and are constrained by electrostatic forces to follow the same quasicircular orbit. A WEP violation [$\delta(A, B) \neq 0$] would result in a difference $-\delta(A, B)\vec{g}$ in the electrostatic feedback forces providing the accelerations needed to maintain the test masses in the same orbit. The satellite can be spun around the normal to the orbital plane and oppositely to the orbital motion in order to increase the frequency of the Earth gravity modulation. In this case, in the satellite frame, the Earth gravity field rotates at the sum of the orbital and spin frequencies (see Fig. 1). A WEP violation would give a signal modulated at this frequency, denoted f_{EP}. The Earth gravity field has a mean amplitude of 7.9 m s^{-2} at 710 km altitude, and testing the WEP with an accuracy of 10^{-15} necessitates measuring the differential constraining force per unit of mass (henceforth called acceleration) between test mass pairs with an 1σ accuracy of 7.9×10^{-15} m s^{-2} at f_{EP}.

SUEP and SUREF use servo loops to keep each test mass motionless with respect to its surrounding silica electrodes, with a relative position resolution of 3×10^{-11} m Hz$^{-1/2}$ measured within the bandwidth [2×10^{-4} Hz, 1 Hz]. The position measurement noise leads to an acceleration noise contribution lower than 2×10^{-14} m s^{-2} Hz$^{-1/2}$ at frequencies $f_{EP} = 3.1113 \times 10^{-3}$ Hz (for SUEP) and $f_{EP} = 0.9250 \times 10^{-3}$ Hz (for SUREF). This is well below the requirement specification of 2×10^{-12} m s^{-2} Hz$^{-1/2}$ at f_{EP} for each instrument. The electrode sets are engraved on silica parts whose positions are very stable with respect to a common silica hat part mounted on a common INVAR sole plate. Electrostatic forces are exerted capacitively on the test masses without any mechanical contact. Thin gold wires of 7 μm diameter are used to control the charge on each test mass.

Both high-frequency (100 kHz [17]) capacitive sensing and low-frequency (<1 Hz) control of each test-mass position and attitude about its 6 degrees of freedom (DOF) are performed by the same set of electrodes. The
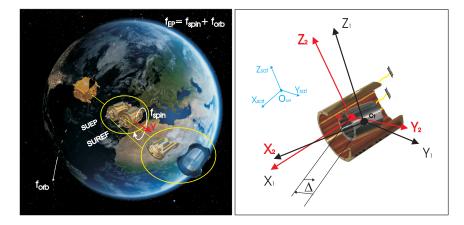

FIG. 1.   Left: The four test mass orbiting around Earth (credit CNES, Virtual-IT 2017). Right: Test masses and satellite frames; the $(X_{sat}, Y_{sat}, Z_{sat})$ triad defines the satellite frame; the reference frames $(X_k, Y_k, Z_k, k = 1, 2)$ are attached to the test masses (black for the inner mass $k = 1$, red for the outer mass $k = 2$); the X_k axes are the test-mass cylinders' longitudinal axis and define the direction of WEP test measurement; the Y_k axes are normal to the orbital plane, and define the rotation axis when the satellite spins; the Z_k axes complete the triads. The 7 μm gold wires connecting the test masses to the common Invar sole plate are shown as yellow lines. $\vec{\Delta}$ represents the test-mass off-centering. The centers of mass correspond to the origins of the sensor-cage-attached reference frames.

position and attitude are derived from the combination of different electrodes' capacitive sensing, then a digital PID (proportional integral derivative) control calculates the necessary voltage to apply to each electrode. For each pair of symmetric electrodes controlling one DOF, the (small) antisymetric voltages applied on the electrodes are super-imposed on a larger dc voltage, thereby making the applied electrostatic forces proportional to first order to the applied voltages. The output of the instrument is thus derived from the applied voltages. In the absence of a WEP violation, and if everything is perfect and aligned (in contrast to the exaggerated case of Fig. 1's right panel), the difference of accelerations of two concentric test masses is expected to vanish whatever their composition or mass. In case of a violation, the difference of accelerations would be directly proportional to the magnitude of Earth's gravitational field.

To improve the measurements, additional servo loops reduce nongravitational accelerations of the satellite for the 6 DOF using cold gas thrusters driven by the accelerometers' measurements of the linear and angular accelerations (similar to LISA Pathfinder [18]). The payload measurements are completed by satellite attitude measurements from the star trackers. The thrusters can also apply additional accelerations to the satellite in order to calibrate the instruments.

During most of the scientific sessions the drag-free loop is controlled by the output of one of the test masses. We have checked that the residual acceleration measurements were below 1.5×10^{-12} m s^{-2} Hz$^{-1/2}$ for this test mass and below 3×10^{-11} m s^{-2} Hz$^{-1/2}$ for the other; this is much better than the requirement on the drag-free and attitude control system (DFACS) of 3×10^{-10} m s^{-2} Hz$^{-1/2}$ about $f_{\rm EP}$. The DFACS limits the acceleration of one of the two instruments (SUEP or SUREF, depending of the session). The other instrument, 17.5 cm away (mainly along the Y axis), undergoes inertial and gravity gradient accelerations which preclude getting the same performance despite the excellent attitude control of the satellite. This is one of the reasons why we conduct independent experiments in different sessions, using either SUREF or SUEP, but not both simultaneously.

The payload is integrated inside a magnetic shield at the center of the microsatellite whose efficiency was modeled with a 3D magnetic tool and with measured magnetic properties on instrument parts. The sensor geometry and the low-noise electronics benefit from the very stable passive thermal cocoon of the satellite.

Measurements and estimation of systematic errors.—We define $\vec{\Gamma}_k$ as the acceleration exerted by the surrounding capacitive sensor cage on the kth test mass. The three components of each acceleration $\vec{\Gamma}_k$ are measured in the frame (X_k, Y_k, Z_k) attached to the corresponding sensor cage (see Fig. 1). Because of small (time-independent) misalignments with respect to the satellite frame $(X_{\rm sat}, Y_{\rm sat}, Z_{\rm sat})$, the locally measured components $\vec{\Gamma}_k$ are related to their components $\vec{\Gamma}_k^{\rm sat}$ in the satellite frame via $\vec{\Gamma}_k = [\theta_k]\vec{\Gamma}_k^{\rm sat}$, where the matrix $[\theta_k]$ reads

$$[\theta_k] = \begin{bmatrix} 1 & \theta_{kz} & -\theta_{ky} \\ -\theta_{kz} & 1 & \theta_{kx} \\ \theta_{ky} & -\theta_{kx} & 1 \end{bmatrix}.$$

The three (antisymmetric) off-diagonal elements θ_{kl} measure the small rotation between the satellite frame and the kth test-mass frame (designed such that $\theta_{kl} < 2.5 \times 10^{-3}$ rad).

Besides the antisymmetric off-diagonal elements θ_{kl} there are also measurement biases, nonunit scale factors, and coupling defects which lead the readouts to measure the components $\vec{\Gamma}_k^{\rm meas} = [A_k]\vec{\Gamma}_k$ where the sensitivity matrix $[A_k]$ reads

$$[A_k] = \underbrace{\begin{bmatrix} 1 + K_{kx} & 0 & 0 \\ 0 & 1 + K_{ky} & 0 \\ 0 & 0 & 1 + K_{kz} \end{bmatrix}}_{\text{scale factor}}$$

$$+ \underbrace{\begin{bmatrix} 0 & \eta_{kz} & \eta_{ky} \\ \eta_{kz} & 0 & \eta_{kx} \\ \eta_{ky} & \eta_{kx} & 0 \end{bmatrix}}_{\text{coupling}}.$$

We then define the common- and differential-mode sensitivity matrices of the two inertial sensors as $[M_c] = \frac{1}{2}([A_1][\theta_1] + [A_2][\theta_2])$ and $[M_d] = \frac{1}{2}([A_1][\theta_1] - [A_2][\theta_2])$. By design, the elements of $[M_d]$ are smaller than 10^{-2} and known to 10^{-4} accuracy after in-orbit estimation. Similarly, $[M_c]$ is close to the identity matrix with a subpercent error.

The quantity of interest is the difference between the accelerations exerted on the two test masses of a given sensor unit, namely, the inner mass $(k = 1)$ and the outer mass $(k = 2)$, $\vec{\Gamma}_d^{\rm meas} \equiv \vec{\Gamma}_1^{\rm meas} - \vec{\Gamma}_2^{\rm meas}$. This measured differential acceleration is directly related to the Eötvös ratio $\delta(2, 1)$ and to the various forces acting on the satellite (see Ref. [19] for a detailed derivation):

$$\begin{aligned} \vec{\Gamma}_d^{\rm meas} \simeq\; & \vec{K}_{0,d} \\ & + [M_c]\{([T] - [{\rm In}])\vec{\Delta} - 2[\Omega]\dot{\vec{\Delta}} - \ddot{\vec{\Delta}} \\ & + \delta(2,1)\vec{g}(O_{\rm sat})\} \\ & + 2[M_d]\vec{\Gamma}_c^{\rm app} + \vec{\Gamma}_d^{\rm quad} + [{\rm Coupl}_d]\dot{\vec{\Omega}} + \vec{\Gamma}_d^n. \quad (1) \end{aligned}$$

All terms in Eq. (1) are described in Table II. Equation (1) shows that the measurement may be sensitive to the common acceleration of the platform applied to both sensors of each instrument. Hence, the mission scenario includes calibration sessions scheduled to match the sensitivities of the sensors, in order to estimate $[M_d]$ and to *a posteriori* correct its effect [20].

TABLE II.   Description of the terms in Eq. (1).

Terms of Eq. (1)	Description of the terms
$\vec{K}_{0,d}$	Vector of the difference of the inertial sensor measurement bias
$\vec{\Delta} = (\Delta_x, \Delta_y, \Delta_z)^T$	Vector (in the satellite frame) connecting the center of the inner mass to that of the outer mass
$\dot{\vec{\Delta}}$ and $\ddot{\vec{\Delta}}$	First and second time derivatives of $\vec{\Delta}$; they are nullified in the instrument's bandwidth when the instrument's servo controls maintain the masses motionless vs the satellite frame
$[\Omega]$	Satellite's angular velocity matrix, $\vec{\Omega} \times \vec{r} = [\Omega]\vec{r}$
$[T]$	Gravity gradient tensor in the satellite frame
$[In]$	Matrix gradient of inertia defined in the satellite frame by $[In] = [\dot{\Omega}] + [\Omega][\Omega]$
$\vec{g} = (g_x, g_y, g_z)^T$	Gravity acceleration vector in the satellite frame of 7.9 m s^{-2} in magnitude at the 710 km altitude
$\delta(2,1)$	Eötvös parameter of the outer mass (2) with respect to the inner mass (1)
$2[\Omega]\dot{\vec{\Delta}}$	Coriolis effect in the satellite frame; very weak because the relative velocity of the test masses at the test frequency is limited by the integral term of the accelerometer servo loops and because the angular velocity is well controlled by the satellite DFACS loops
$\vec{\Gamma}_c^{\text{app}}$	Mean acceleration applied on both masses in the satellite frame; limited by the satellite DFACS
$\vec{\Gamma}_d^{\text{quad}}$	Difference of the nonlinear terms in the measurement, mainly the difference of the quadratic responses of the inertial sensors
$[\text{Coupl}_d]$	Matrix of the difference, between the two sensors, of the coupling from the angular acceleration $\dot{\vec{\Omega}}$ to the linear acceleration
$\vec{\Gamma}_d^n$	Difference of the acceleration measurement noises of the two sensors (coming from thermal noise, electronics noise, parasitic forces, etc.), comprising stochastic and systematic error sources

The gravity acceleration $\vec{g}$ and the gravity gradient tensor $[T]$ projected into the satellite frame are computed from the ITSG-GRACE2014s Earth's gravity potential model [19], by using the measured position and attitude of the satellite. The distance between the two test masses' centers of mass is estimated to be $(\Delta_x, \Delta_y, \Delta_z) = (20.1, -8.0, -5.6) \pm (0.1, 0.2, 0.1)$ μm. The Δ_x and Δ_z components are estimated from the gravity gradient signal at $2f_{\text{EP}}$ (at $2f_{\text{EP}}$, systematic errors are smaller than 8×10^{-14} m s^{-2}, much smaller than required for the above 0.1 μm accuracy). The corresponding acceleration is simultaneously computed and corrected from the measured

differential acceleration. The Δ_y component, although contributing only marginally to the differential acceleration, is estimated through a dedicated session [20]. In the particular mode where the satellite is spinning, the effect of test-mass miscentering is negligible at f_{EP} and could be left uncorrected. The satellite orbit and attitude are determined to 0.42 m and 0.4 μrad precision, much better than the required 2 m and 1 μrad.

The different error source contributions to Eq. (1) are summarized in Table III [21,22]. As X is the preferred axis for the EP test, in-flight calibration of the first-row coefficients of $[M_d]$ is sufficient: $M_{dxx} = 8.5 \times 10^{-3} \pm 1.5 \times 10^{-4}$,

TABLE III.   Evaluation of systematic errors in the differential acceleration measurement for SUEP at $f_{\text{EP}} = 3.1113 \times 10^{-3}$ Hz.

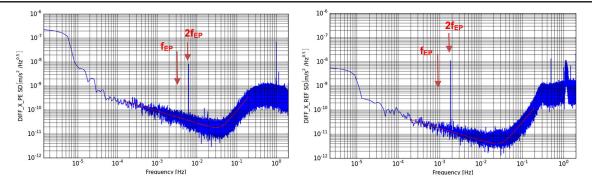| Term in the Eq. (1) projected on $\vec{x}$	Amplitude or upper bound	Method of estimation
Gravity gradient effect $[T]\vec{\Delta}$ along X @ f_{EP} (in phase with g_x)		
$(T_{xx}\Delta x; T_{xy}\Delta y; T_{xz}\Delta z)$	$<(10^{-18}; 10^{-19}; 10^{-17})$ m s^{-2}	Earth's gravity model and in flight calibration
Gradient of inertia matrix [In] effect along X at f_{EP}		
$\dot{\Omega}_y\Delta_z - \dot{\Omega}_z\Delta_y$	10^{-18} m s^{-2}	DFACS performances and calibration
$\Omega_x\Omega_y\Delta_y - \Omega_x\Omega_z\Delta_z - (\Omega_y^2 + \Omega_z^2)\Delta_x$	1.3×10^{-17} m s^{-2}	DFACS performances and calibration
Drag-free control		
$([M_d]\vec{\Gamma}_c^{\text{app}}) \cdot \vec{x}$	1.7×10^{-15} m s^{-2}	DFACS performances and calibration
Instrument systematics and defects		
$(\vec{\Gamma}_d^{\text{quad}}) \cdot \vec{x}$	5×10^{-17} m s^{-2}	DFACS performances and calibration
$([\text{Coupl}_d]\dot{\vec{\Omega}}) \cdot \vec{x}$	$<2 \times 10^{-15}$ ms^{-2}	Couplings observed during commissioning phase
Thermal systematics	$<67 \times 10^{-15}$ m s^{-2}	Thermal sensitivity in-orbit evaluation
Magnetic systematics	$<2.5 \times 10^{-16}$ m s^{-2}	Finite-element calculation
Total of systematics in $\Gamma_{dx}^{\text{meas}}$	$<71 \times 10^{-15}$ m s^{-2}	
Total of systematics in δ	$<9 \times 10^{-15}$	

FIG. 2.　Square root of the measured PSD of the differential acceleration along X during the scientific session 218 with SUEP (left) and during the scientific session 176 with SUREF (right); on left, $f_{EP} = 3.1113 \times 10^{-3}$ Hz, $f_{orb} = 1.6818 \times 10^{-4}$ Hz and satellite spin $= 2.9432 \times 10^{-3}$ Hz; on right, $f_{EP} = 0.9250 \times 10^{-3}$ Hz and satellite spin $= 0.5886 \times 10^{-3}$ Hz; the gravity gradient effect are clearly observed at $2f_{EP}$. The red line is a power-law fit to the spectrum.

$|M_{dxy}|$ and $|M_{dxz}| < 1.5 \times 10^{-4}$ rad. The effect of Earth's gravity field and its gradient is considered along X at f_{EP} and in phase with any EP signal. All other terms are considered at f_{EP} but without considering the phase which is conservative.

Thermal effects are currently the dominant contribution to the systematic error. These were evaluated in a specific session where thermistors applied temperature variations at f_{EP} either to the electronic interface (ΔT_{FEEU}) or to the SU baseplate (ΔT_{SU}). The effect of these variations (or their gradients) on the differential acceleration signal is $\Gamma_{dx}^{meas}(\text{therm}) = (7 \times 10^{-11} \, \text{ms}^{-2}\text{K}^{-1})\Delta T_{FEEU} + (4.3 \times 10^{-9} \, \text{ms}^{-2}\text{K}^{-1})\Delta T_{SU}$. The SU temperature sensitivity was more than 2 orders of magnitude larger than expected and far too large to be due to the radiometer effect or radiation pressure [23] and thus must come from another source. Fortunately the maximum observed FEEU and SU temperature variations during 120 orbits were less than, respectively, 20×10^{-6} K and 15×10^{-6} K, about 2 orders of magnitude smaller than expected. The mean variation in fact was limited by the resolution of the probes, leading to the upper limit on the thermal systematic included in Table III. Additional data could lower this upper limit.

The self gravity and magnetic effects have been evaluated by finite element calculation and found negligible compared to the previous error sources.

Figure 2 shows the measurement spectrum for SUEP and SUREF. As expected, the measured noise varies as f^2 at high frequency; at low frequency, it varies as the $f^{-1/2}$ law expected for the damping noise of the gold wire. At f_{EP} the noise of the differential acceleration is dominated by this damping noise. It amounts to $5.6 \times 10^{-11} \, \text{m s}^{-2} \, \text{Hz}^{-1/2}$ for SUEP and to $1.8 \times 10^{-11} \, \text{m s}^{-2} \, \text{Hz}^{-1/2}$ for SUREF.

In the data used for this Letter, the total amplitude of the differential acceleration FFT appears dominated by statistical signals over integration times lower than 62 to 120 orbits, respectively, for SUREF and SUEP, as shown in Fig. 3: the blue line shows the evolution of the FFT amplitude at f_{EP} as the integration time (i.e., number of orbits N) increases; the red line shows a $N^{-1/2}$ fit. The total FFT amplitude evolution appears inversely proportional to the square root of the integration time. A steady systematic effect would break this inverse proportionality law; for example a steady systematic effect (including a potential EP signal in SUEP) would show up as a constant offset.
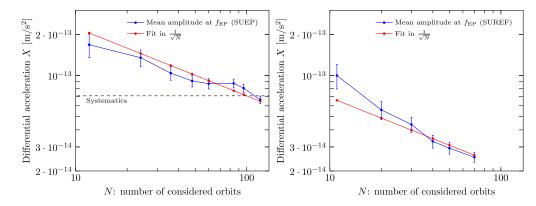

FIG. 3.　Evolution of the mean amplitude of the FFT of the differential signal along X at f_{EP} as a function of integrating times (on left, from 12 to 120 orbits for the session 218 with SUEP and on right, from 11 to 62 orbits for SUREF). The mean of the FFT is computed as the average of the Fourier amplitudes over a narrow band of 10^{-4} Hz around f_{EP}. For SUEP, the black dashed line shows the estimated upper bound of the systematic errors given by the error assessment of Table III.

The results from both SUEP and SUREF are reaching sensitivities close to where no time dependent systematic effects should become apparent if they are present (without counterbalancing signal in SUEP) at the upper limit to the predictions shown in Table III.

Eötvös parameter estimation.—We simultaneously estimate the Eötvös parameter $\delta(2,1)$ and the Δ_x and Δ_z miscenterings with a least-squares fit based on Eq. (1) in the frequency domain. More precisely, N equations (one per data point) in the time domain are converted into N equivalent equations in the frequency domain through a Fourier transform; then the equation system is lightened by selecting the bands where the signal is expected (centered on f_{EP} for $\delta(2,1)$ and $2f_{EP}$ for $\Delta_{x,z}$, with a 4×10^{-5} Hz width [24]). The 1σ statistical errors are given by the 1σ uncertainty on the least-squares estimate. The SUEP systematic error 9×10^{-15} is given by the upper limit evaluation performed in Table III.

The Eötvös parameter for the SUEP instrument is obtained with 120 orbits (713 518 s):

$$\delta(\mathrm{Ti}, \mathrm{Pt}) = [-1 \pm 9(\mathrm{stat}) \pm 9(\mathrm{syst})] \times 10^{-15} \quad \text{at } 1\sigma, \quad (2)$$

with a goodness-of-fit parameter $\chi^2_{\mathrm{red}} = 1.17$

The test performed with the SUREF instrument over 62 useful orbits (368 650 s) yields

$$\delta(\mathrm{Pt}, \mathrm{Pt}) = [+4 \pm 4(\mathrm{stat})] \times 10^{-15} \quad \text{at } 1\sigma, \quad (3)$$

with $\chi^2_{\mathrm{red}} = 1.24$. This estimation is fully compatible with a null result (which is expected for this instrument), suggesting no evidence of systematic errors at the order of magnitude of 4×10^{-15} consistent with the SUEP conservative evaluation of Table III. To complete this analysis on the SUREF, specific sensitivity sessions are scheduled before the end of the mission in particular to detail the systematics.

Conclusion.—We have presented the first results on *MICROSCOPE*'s test of the weak equivalence principle with conservative upper limits for some errors. Nevertheless this result constitutes an improvement of one order of magnitude over the present ground experiments [2]. Forthcoming sessions dedicated to complete the detailed exploration of systematic errors will allow us to improve the experiment's accuracy. Thousands of orbits of scientific measurements should be available by the end of the mission in 2018. The integration over longer periods of the differential accelerometer signal should lead to a better precision on the WEP test. *MICROSCOPE* will certainly take a step forward in accuracy, closer to the mission objective of 10^{-15} and bring new constraints to alternative gravity theories.

*Pierre.Touboul@onera.fr
†Gilles.Metris@oca.eu
‡Manuel.Rodrigues@onera.fr

[1] L. Eötvös, D. Pekár, and E. Fekete, Beiträge zum Gesetz der Proportionalität von Trägheit und Gravität, Ann. Phys. (Berlin) **68** (1922); Annales Universitatis Scientiarium Budapestiensis de Rolando Eötvös Nominate, Sectio Geologica **7**, 111 (1963).

[2] T. A. Wagner, S. Schlamminger, J. H. Gundlach, and E. G. Adelberger, Torsion-balance tests of the weak equivalence principle, Classical Quantum Gravity **29**, 184002 (2012).

[3] J. G. Williams, S. G. Turyshev, and D. H. Boggs, Lunar laser ranging tests of the equivalence principle, Classical Quantum Gravity **29**, 184004 (2012).

[4] A. Einstein, Über das Relativitätsprinzip und die aus demselben gezogene Folgerungen, Jahrb. Radioakt. Elektron. **4**, 411 (1907).English translation in A. Beck and P. Havas, *The Collected Papers of Albert Einstein* (Princeton University Press, Princeton, NJ, 1989), Vol. 2, doc. 47.

[5] A. Einstein, Die grundlage der allgemeinen relativitätstheorie, Ann. Phys. (Berlin) **49**, 252 (1916); English translation in A. Engel and E. Schucking, *The Collected Papers of Albert Einstein* (Princeton University Press, Princeton, NJ, 1989), Vol. 6, doc. 30.

[6] C. M. Will, The confrontation between general relativity and experiment, Living Rev. Relativity **17**, 146 (2014).

[7] B. P. Abbott *et al.*, Observation of Gravitational Waves from a Binary Black Hole Merger, Phys. Rev. Lett. **116**, 061102 (2016).

[8] T. Damour and A. M. Polyakov, The string dilaton and a least coupling principle, Nucl. Phys. **B423**, 532 (1994).

[9] T. Damour, F. Piazza, and G. Veneziano, Runaway Dilaton and Equivalence Principle Violations, Phys. Rev. Lett. **89**, 081601 (2002).

[10] J. Khoury and A. Weltman, Chameleon Fields: Awaiting Surprises for Tests of Gravity in Spaces, Phys. Rev. Lett. **93**, 171104 (2004).

[11] P. Fayet, Extra U(1)'s and new forces, Nucl. Phys. **B347**, 743 (1990).

[12] P. Fayet, The light *U* boson as the mediator of a new force, coupled to a combination of Q, B, L and dark matter, Eur. Phys. J. C **77**, 53 (2017).

[13] P. Touboul, M. Rodrigues, G. Métris, and B. Tatry, *MICROSCOPE*, testing the equivalence principle in space, C. R. Acad. Sci. Paris Ser. IV **2**, 1271 (2001).

[14] P. Touboul, G. Métris, V. Lebat, and A. Robert, The *MICROSCOPE* experiment, ready for the in-orbit test of the equivalence principle, Classical Quantum Gravity **29**, 184010 (2012).

[15] A. Connes, T. Damour, and P. Fayet, Aspherical gravitational monopoles, Nucl. Phys. **B490**, 391 (1997).

[16] E. Willemenot, PhD Thesis, Orsay, 1997.

[17] V. Josselin, P. Touboul, and R. Kielbasa, Capacitive detection scheme for space accelerometers applications, Sens. Actuators A **78**, 92 (1999).

[18] M. Armano *et al.*, Sub-femto-g Free Fall for Space-Based Gravitational Wave Observatories: LISA Pathfinder Results, Phys. Rev. Lett. **116**, 231101 (2016).

[19] T. Mayer-Gurr, A. Eicker, and K. H. Ilk, in Proc. First Symp. Int. Grav. Field Ser., ITG-GRACE02s: A GRACE Gravity Field Derived from Short Arcs of the Satellites Orbit (Elsevier, Amsterdam, 2006).

[20] E. Hardy, A. Levy, M. Rodrigues, P. Touboul, and G. Métris, Validation of the in-flight calibration procedures for the *MICROSCOPE* space mission, Adv. Space Res. **52**, 1634 (2013).

[21] P. Touboul, The *MICROSCOPE* mission and its uncertainty analysis, Space Sci. Rev. **148**, 455 (2009).

[22] P. Touboul *et al.*, Space test of the equivalence principle: First results of the *MICROSCOPE* mission, Classical Quantum Gravity (to be published).

[23] L. Carbone, A. Cavalleri, G. Ciani, R. Dolesi, M. Hueller, D. Tombolato, S. Vitale, and W. J. Weber, Thermal gradient-induced forces on geodesic reference masses for LISA, Phys. Rev. D **76**, 102003 (2007).

[24] E. Hardy, A. Levy, G. Métris, M. Rodrigues, and P. Touboul, Determination of the equivalence principle violation signal for the *MICROSCOPE* space mission: Optimization of the signal processing, Space Sci. Rev. **180**, 177 (2013).